HiSST: 2nd International Conference on
High-Speed Vehicle Science & Technology
20-24 April 2020, Bruges, Belgium

Numerical Modelling of Cavity Enhanced Jet Interactions in a Scramjet

Tim Roos[1], Adrian S. Pudsey[2], Hideaki Ogawa [3], Mathew G. Bricalli [4]

Abstract

Cavities have been widely studied for mixing, flameholding and ignition enhancement in scramjet combustors. When used for this purpose, the cavity is commonly placed downstream of the fuel injector and the cavity flowfield is unsteady in nature. Recently, a novel arrangement where the cavity placed upstream of the injector has been proposed for mixing enhancement, and there is some evidence that the associated flowfield is steady. The present study compares Reynolds-averaged Navier-Stokes (RANS) and unsteady RANS (URANS) simulations of the upstream cavity arrangement to assess the stability of the flowfield and the ability of RANS to capture the one-dimensional performance of the flowfield. It is found that the cavity flowfield is steady in nature, because the primary mechanism that drives self-sustained oscillation in conventional cavity flow is absent in the upstream cavity arrangement. Both simulation approaches also result in near identical predictions of key performance variables and flowfield behaviour, demonstrating that one-dimensional mixing performance and the flowfield characteristics of the upstream cavity geometry can be adequately captured using RANS.

Keywords: *Upstream cavity, Computational Fluid Dynamics, URANS, Jet interaction, Fuel mixing*

Nomenclature

Latin
d – Injector diameter
f – Frequency
h – Altitude
k – Measure of vortex convection speed
m – Oscillation mode
p – Pressure
q – Dynamic pressure
u – Streamwise velocity
y^+ – Normalised wall distance
D – Cavity depth
L – Cavity length
L/D – Cavity aspect ratio
M – Mach number
Re – Reynolds number
Str – Strouhal number
T – Temperature
Y_p – Vertical jet centre of mass

Greek
α – Species mass fraction, constant
γ – Ratio of specific heats
η_{mixing} – Mixing efficiency
ρ – Density
τ – Time

Subscripts
∞ – Freestream
j – Jet
t – Total

1. Introduction

Cavities are commonly used in scramjet combustors to enhance ignition and provide flameholding. When used for this purpose they are generally placed at various distances downstream of the fuel injector, to ensure a continuous supply of fuel to the cavity and facilitate continuous combustion inside the cavity.

[1] *School of Engineering, RMIT University, Melbourne, Australia, timnmnroos@gmail.com*
[2] *School of Engineering, RMIT University, Melbourne, Australia, adrian.pudsey@rmit.edu.au*
[3] *Department of Aeronautics and Astronautics, Kyushu University, Fukuoka, Japan, hideaki.ogawa@aero.kyushu-u.ac.jp*
[4] *School of Engineering, RMIT University, Melbourne, Australia, mathew.bricalli@rmit.edu.au*

When a cavity is exposed to a supersonic cross flow an unsteady, oscillating shock structure can develop [6, 7, 8, 21, 24], depending on the length-to-depth ratio (L/D) of the cavity [3]. If $2-3 < L/D < 10-12$ the cavity shear layer spans the length of the cavity (termed open cavity flow) and self-sustained oscillations develop inside the cavity, whereas for $L/D > 13$ the shear cavity shear layer attaches to the cavity floor before separating and attaching downstream of the cavity aft wall (termed closed cavity flow), preventing self-sustained oscillation. Since closed cavities incur a larger drag penalty and feature higher wall heat flux than open cavities, open cavities are most commonly used in scramjets.

Figure 1 shows the feedback mechanism that drives the self-sustained oscillations in open cavity flow. As the cavity shear layer oscillates around the junction between the aft wall and the combustor wall, periodic shock and expansion waves form inside of and around the cavity. When the shear layer impinges on the cavity aft wall mass is added to the cavity and a compression wave propagates to the front of the cavity, deflecting the shear layer up as it bounces off the cavity front wall. The deflection in the cavity shear layer is convected downstream and the shear layer is lifted over the cavity aft wall, incurring an oblique shock in the freestream flow and removing mass from the cavity. As the shear layer deflects down again the feedback loop is complete and the oscillations is sustained.

Heller et al. [8] proposed the following equation to calculate the frequency of the cavity oscillations, which is a modified version of the equation proposed by Rossiter [20] to account for compressibility effects:

$$f_m = \frac{Str \cdot u_\infty}{L} = \frac{m-\alpha}{\{M_\infty/\sqrt{1+[(\gamma_\infty-1)/2]M_\infty^2}+1/k\}} \cdot \frac{u_\infty}{L} \tag{1}$$

where m is the oscillation mode, α is a constant, M_∞ is the freestream Mach number, k is a measure of vortex convection speed, U_∞ is the freestream velocity, L is cavity length and γ_∞ is the specific heat ratio in the freestream. The values of α and k depend on the flowfield, however values of $\alpha = 0.25$ and $k = 0.57$ show good agreement with experiments [8] .

The oscillations described above make the open cavity flowfield unsteady in nature, requiring supersonic combustor flowpaths with open cavities to be modelled using computationally expensive time-accurate simulation approaches such as Large Eddy Simulation (LES) that capture this unsteadiness to obtain accurate results. The high computational cost limits the size of parametric studies comparing the performance of a range of cavity geometries or arrangement, complicating combustor design.

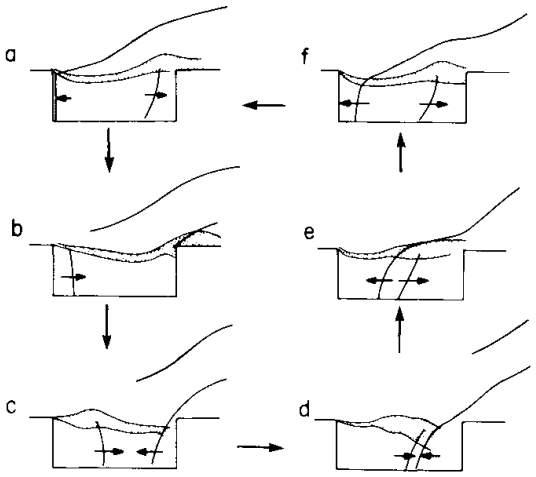

Fig 1. Visualisation of the cavity oscillation process. From [7].

Recently a new combustor arrangement, where a cavity is placed directly upstream of the fuel injection

point, has been explored by these authors [17, 19, 18]. It was observed that in the upstream cavity flowfield the cavity shear layer is lifted over the aft wall of the cavity, removing a key component of the feedback mechanism driving oscillations, Fig. 1. In addition, the study considered a Mach 4.3 freestream and there is experimental evidence that at Mach numbers in excess of 3.2 large-scale self-sustained oscillations disappear [25, 1]. This suggests that the upstream cavity flowfield could be steady in high supersonic Mach number flows, allowing the use of RANS to cheaply evaluate upstream cavity performance.

The purpose of the present paper is to compare RANS and URANS simulations of the newly proposed upstream cavity arrangement to assess the stability of the flowfield and determine the ability of RANS to accurately capture the flowfield, both in terms of flow physics and in terms of one-dimensional flowfield performance. The effect of time-accurate modelling on the cavity flowfield and several one-dimensional performance parameters is studied in detail and the temporal stability of the flowfield is analysed.

2. Method

2.1. Flow Solver

The commercial solver CFD++ was used for all calculations [5] in this work. The code uses a unified grid framework, facilitating unified treatment of a number of cell types in both fully structured, unstructured or hybrid grid topologies. Multi-dimensional Total Variation Diminishing (TVD) polynomials are used to discretise inviscid fluxes and cell interface fluxes are calculated using a compressible Riemann solver.

All calculations were set up using the 13 species, 33 reaction H_2 - Air scheme of Jachimowski [9], however the reactions were not activated in the current study hence the flow is chemically frozen. Turbulence was modelled using Menter's 2003 two-equation Shear Stress Transport (SST) k-ω model [14, 23]. The SST model utilises the k-ω formulation close to the wall, blending to the k-ε model towards the freestream. This model is less sensitive to specification of freestream turbulence level compared to the k-ω model and performs comparatively well in adverse pressure gradients and separated flows. The SST model has previously also been used in other supersonic flow cavity studies [2, 13, 17, 19, 18].

For the URANS simulation an implicit, second order time and space accurate scheme was used and the dual time stepping convergence acceleration scheme that is available within CFD++ was used for the first 35 time steps, during flow stabilisation. More details can be found in [5].

The global time step was set to $\Delta\tau = 3 \times 10^{-6}$ s. Using the modified Rossiter formula [8], Eq. (1), the first three harmonic frequencies of the cavity are predicted to be 20.8 kHz, 48.5 kHz and 76.3 kHz, respectively, yielding an oscillation period of 1.31×10^{-5} s for the third oscillation mode. The third oscillation mode is therefore sampled at least 4 times using a time step of $\Delta\tau = 3 \times 10^{-6}$ s which is considered sufficient for this study. The total simulation time was $\tau = 3 \times 10^{-4}$ s, in excess of the establishment time for self-sustained oscillation which is calculated to be $\tau = 1.29 \times 10^{-5}$ s using the relation from [26].

For the RANS simulation a steady state implicit scheme with second order accuracy in space was used. Both the RANS and URANS simulations were initiated from a set of initial conditions that represent fuel about to issue from the injector and no established recirculation inside the cavity.

2.2. Geometry and Mesh

The domain for this study was modified from the geometry used in [17, 19] and is shown in Fig. 2. The domain comprises a flat plate with a single circular injector of diameter d_j = 2 mm and a cavity placed 1.5 mm upstream of the injector origin. The cavity has a length L = 24 mm and a depth D = 1.6 mm, or L/d_j = 12 and D/d_j = 0.8 when normalised by the injector diameter. The length of the flat plate downstream of the injector was set to 20 mm and a full injector was modelled (in contrast to [19] where only one half of the injector was modelled) to capture any periodicity in the flowfield. The freestream enters from the left.

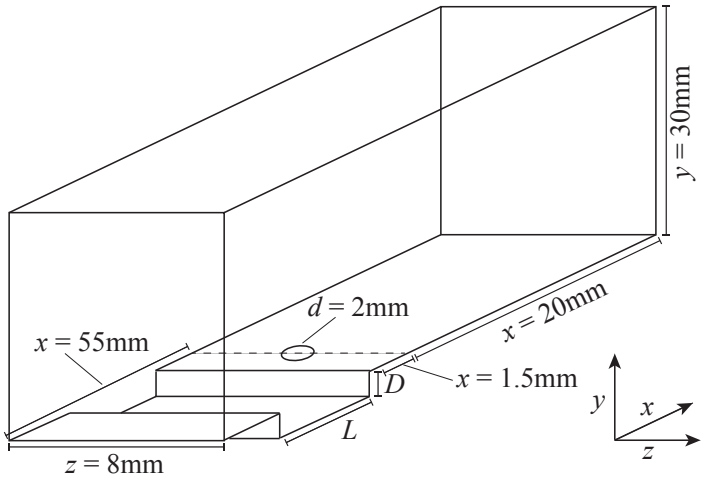

Fig 2. Geometry of the configuration used in this study (not to scale)

The grid for this study was generated with the commercial grid generation tool Pointwise [15] and was structured in all three directions. First cell height on the combustor wall was set to 1×10^{-3} mm to attain a y^+ value of approximately 1.0 and a hyperbolic tangent function is used to distribute cells in the wall-normal direction. The same wall clustering is used inside the cavity, with the exception of the cavity aft wall; a finer mesh is applied there due to its proximity to the injector. A closeup of the half-injector grid with identical spacing can be found in [19].

2.3. Flow and Boundary Conditions

The inflow conditions for this study are representative of a vehicle with the following flight conditions: altitude $h = 38.4$ km; Mach number $M = 8.4$; dynamic pressure $q = 17.0$ kPa. This leads to combustor inflow conditions of static pressure $p_\infty = 78.8$ kPa, static temperature $T_\infty = 835$ K, velocity $u_\infty = 2468$ m/s and Mach number $M_\infty = 4.33$ [11], with the subscript ∞ referring to combustor freestream conditions. The conditions correspond to those used in scramjet-based shock tunnel studies performed by [10] and yield a unit Reynolds number of Re $= 21.85 \times 10^6$ m^{-1}.

A supersonic inflow profile with a 5 mm boundary layer was specified as the freestream inflow, generated on a two-dimensional flat plate with the same vertical grid point distribution as the combustor domain. More details can be found in [19]. Centroidal extrapolation (*i.e.* no conditions prescribed) was applied to the streamwise outflow and top boundaries, to remove reflecting shocks. The stagnation pressure and temperature were specified for the injector inflow and the injector wall was modelled as an inviscid wall with surface tangency. The flow within the the injector pipe is assumed to be inviscid to relax grid requirements in that region [16]. The turbulence level in the injector was set to 3% with a turbulence length scale of 0.01 m and the injector plenum was not modelled, again following results from [16]. The flat plate and cavity walls were modelled as isothermal 1800 K walls and all wall boundary conditions were solved directly to the wall, so no wall model was used. Periodic boundaries were prescribed on the lateral boundaries for the URANS simulation, while symmetry planes were applied for the RANS simulation to maintain consistency with previous work [17, 19].

A commonly used parameter in supersonic injection studies is the jet-to-freestream momentum ratio I, defined as:

$$I = \left(p\gamma M^2\right)_j / \left(p\gamma M^2\right)_\infty . \tag{2}$$

where p is the static pressure, M is the Mach number and γ is the ratio of specific heats. The subscripts refer to the *jet* (j) or *combustor entry* (∞) conditions. For this study the injector inflow conditions were

set to a total pressure of $p_t = 2.48$ MPa and a total temperature of $T_t = 313$ K, corresponding to $I = 0.84$ and a baseline injector mass flow of 4.7×10^{-3} kg/s.

2.4. Numerical accuracy

An extensive grid convergence study was performed in [17], following the procedure outlined by [4]. An extensive turbulence sensitivity and numerical validation study were also conducted in [17] and the reader is referred to that source for more information. In summary, a grid convergence index (GCI) of 2.42% was obtained for the half-injector grid with and identical grid and the value of mixing efficiency at $x/d = 3$ was found to asymptotically approach the extrapolated value, Fig. 3, indicating that the results are sufficiently independent of the grid.

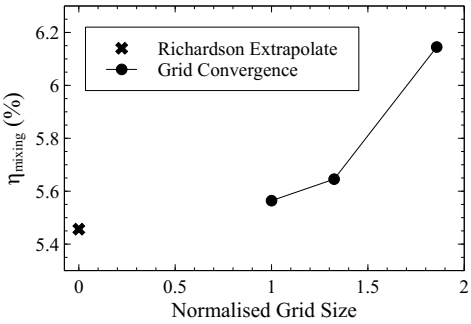

Fig 3. Richardson extrapolation of the mixing efficiency of H_2 at $x/d = 3$.

2.5. Performance parameters

This section will introduce the performance variables that will be used to analyse the results. For all performance variables the two-dimensional integral in the definition is performed over a range of streamwise (yz) slices to obtain the evolution of the performance parameter through the domain.

The mixing efficiency is computed to quantify the degree of mixing in each case. The mixing efficiency is taken from [12] and is defined such that it is an indicator of combustion: any fuel that is locally below the stoichiometric mass fraction (and hence would fully react in a chemically reacting flow) is considered fully mixed, i.e. a mixing efficiency of 1. If the fuel mass fraction locally exceeds the stoichiometric ratio, only the mass fraction of fuel that can fully react using the locally available oxygen (i.e. only some portion of the total local fuel mass fraction) is considered mixed. As the local fuel mass fraction goes to 1, the mixing efficiency therefore progressively goes to 0. To quantify this criterion, the fuel mass fraction that is available for combustion $\alpha^r_{H_2}$ is calculated as:

$$\alpha^r_{H_2} = \begin{cases} \alpha_{H_2} & \alpha_{H_2} \leq \alpha^{st}_{H_2} \\ \left(\frac{1-\alpha_{H_2}}{1-\alpha^{st}_{H_2}}\right) \alpha^{st}_{H_2} & \alpha_{H_2} > \alpha^{st}_{H_2} \end{cases} \tag{3}$$

where $\alpha^{st}_{H_2}$ is the stoichiometric ratio for hydrogen, taken as $\alpha^{st}_{H_2} = 0.0292$, and α_{H_2} is the local fuel mass fraction. The mixing efficiency is then defined as [12]:

$$\eta_{mixing} = \frac{\iint \rho u \alpha^r_{H_2} \, \mathrm{d}A}{\iint \rho u \alpha_{H_2} \, \mathrm{d}A} \tag{4}$$

where ρ is the local density, u the axial velocity and $\alpha^r_{H_2}$ is the fuel mass fraction available for combustion .

To assess the pressure losses due to injection and the introduction of a cavity, the total pressure throughout the domain is computed for each case. Since the top of the domain is modelled as an outflow the

total pressure at a given location has two components: the mass-averaged total pressure through a streamwise slice at that location and the mass-averaged total pressure that has been lost through the top of the domain up to that location. If the second component is not accounted for any mass that leaves through the top plane is incorrectly counted as total pressure loss, while it would still be part of the flow if the top plane were modelled as a wall and it is therefore not a flow-induced total pressure loss. The mass-averaged total pressure on a slice is therefore calculated as:

$$p_t = \frac{\iint p_t \rho |u| \, \mathrm{d}y \, \mathrm{d}z}{\iint \rho |u| \, \mathrm{d}y \, \mathrm{d}z} + \left. \frac{\int_{-55}^{x} \int p_t \rho u \, \mathrm{d}z \, \mathrm{d}x}{\int_{-55}^{x} \int \rho u \, \mathrm{d}z \, \mathrm{d}x} \right|_{y=60} \tag{5}$$

where p_t is the total pressure and the other variables are common with Eq. (4). In the present study, the total pressure loss is calculated by normalising the mass-averaged total pressure on a plane by the freestream total pressure on the combustor inflow plane, $p_{t,\infty} = 26,436,022$Pa .

In addition to the mixing efficiency, vertical penetration of the fuel jet into the freestream is an important factor in assessing the combustion potential of a flow. Increased jet penetration allows for the fuel to reach a larger volume of the combustor and will enable more widespread combustion and heat release, improving combustor performance. In the present work the vertical penetration of the fuel jet is assessed by computing the location of the jet centre of mass above the wall, defined as

$$Y_p = \frac{\iint \rho u \alpha_{\mathrm{H_2}} y \, \mathrm{d}A}{\iint \rho u \alpha_{\mathrm{H_2}} \, \mathrm{d}A} \tag{6}$$

where y is the distance normal to the combustor wall in mm and the other variables are common with Eq. (4).

3. Results

3.1. Temporal Stability

Before analysing the flowfield and one-dimensional performance parameters it is useful to assess the stability of the flowfield. For this purpose Fig. 4 shows static pressure as a function of time at four locations around the cavity on the cavity centreline. Three locations are near the cavity walls, whereas the fourth location is in the cavity centroid.

The figure shows that once the flow has established static pressure at all four locations is constant and no oscillations are present inside the cavity. This is a strong indicator that the flowfield is steady. Near the cavity front wall pressure is decreasing slightly over time, however it is approaching a constant value. The flow establishment time is observed to be ~ 0.16 ms, which is 31 µs higher than the analytically predicted value of 0.129 ms. The discrepancy is likely because of the relatively high cavity aspect ratio; it takes some time for the pressure field to be communicated throughout the cavity and the relation in [26] was developed for open cavities with $L/D = 3$. If the cavity front wall pressure trace is neglected the flow establishment time is ~ 0.135 ms, which is much closer to the predicted value. In the aggregate the analytical expression provides a reasonable estimate of flow establishment time, even though the cavity flow in the current study is markedly different from the investigation the relation is based on.

To examine why no large scale unsteadiness is observed Fig. 5 shows contours of Mach number on the centreplane at solution time $\tau = 3 \times 10^{-4}$ s. Fluid streamlines have been included in the figure to visualise the flowfield around the cavity. The fluid streamlines show that the cavity recirculation region has risen out of the cavity, effectively creating an aerodynamic ramp in front of the injector and shielding the fuel jet from the freestream flow. Because the recirculation region rises out of the cavity the cavity shear layer is lifted over the aft wall; this removes the primary oscillation mechanism in conventional

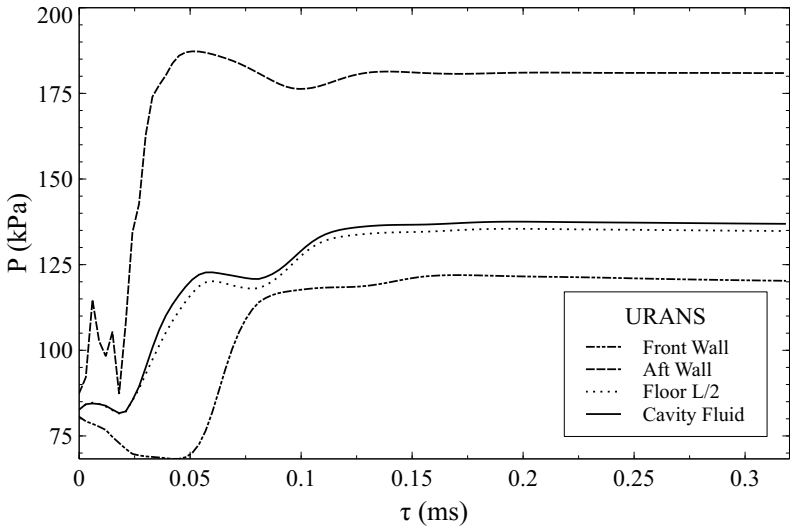

Fig 4. Static pressure as a function of time at four locations inside the cavity, on the cavity centreline.

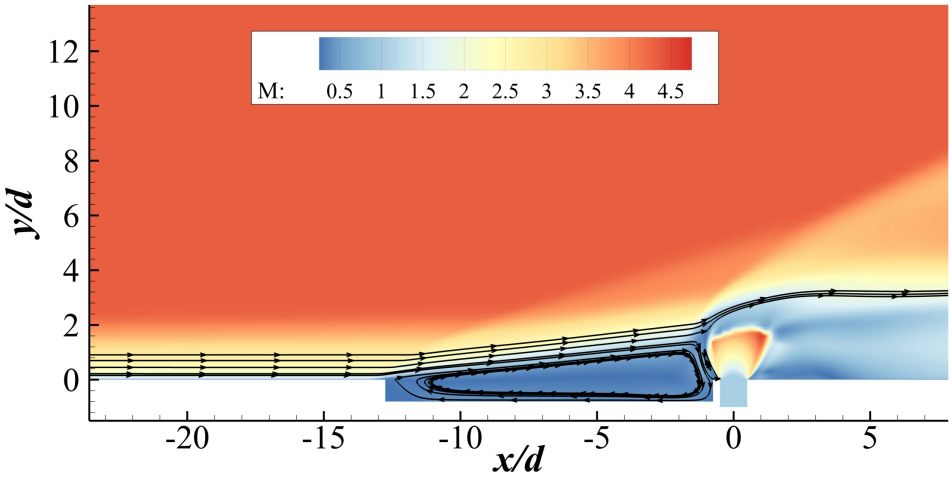

Fig 5. Contours of Mach number on the centreplane at $\tau = 3 \times 10^{-4}$ s.

open cavity flow, and the results of the present study indicate that this removes large scale unsteadiness from the cavity flowfield.

In the conventional cavity flowfield instability in the cavity shear layer is a key process in the self-sustained oscillation mechanism. In the upstream cavity flowfield there is no observable unsteadiness inside the shear layer, as demonstrated by Fig. 6. The figure shows static pressure as a function of time at two locations in the cavity shear layer at $x/d = -2$, near the aft wall of the cavity. Towards the aft wall of the cavity the shear layer has had time to develop and any instability would have been expressed, so the absence of unsteadiness further indicates that the cavity flowfield is steady in nature. The stability of the shear layer can be attributed to the higher supersonic Mach number of the flow, where shear layer entrainment is suppressed because of the high convective Mach number [22].

3.2. Performance Parameters

The effect of numerical modelling approach on the one-dimensional performance of the flowfield is now examined. Three one-dimensional performance parameters are analysed, defined in Section 2.5:

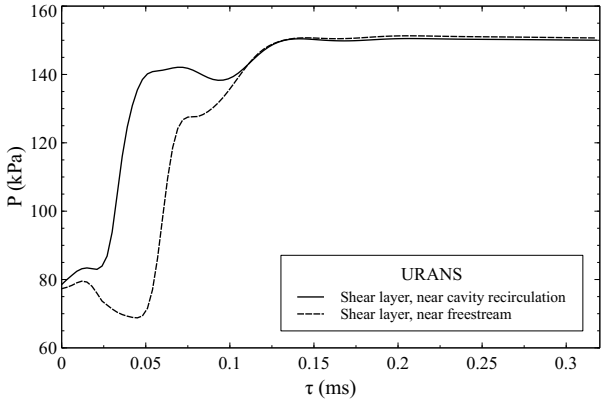

Fig 6. Static pressure at two points inside the cavity shear layer as a function of time. The data is obtained at $x/d = -2$ towards the upper and lower boundary of the shear layer.

mixing efficiency, total pressure loss and jet penetration. For each performance variable the trend obtained from the RANS simulation is displayed together with trends obtained at three time steps in the URANS simulation, taken after the flow has established. To clearly distinguish the RANS simulation, the markers for the RANS trends (termed steady in the figures) have been coloured red.

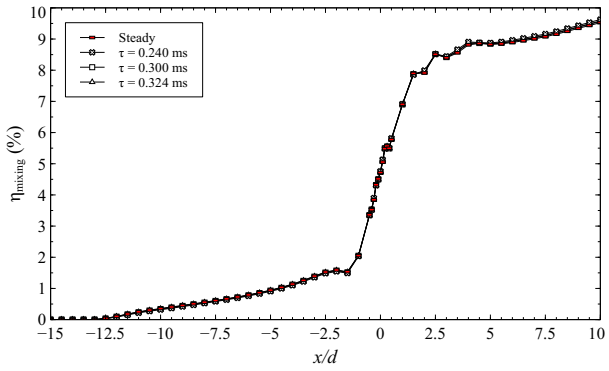

Fig 7. Mixing efficiency through the domain for three timesteps and the steady case.

Figure 7 shows trends of mixing efficiency through the domain. To more closely inspect the difference between the RANS and URANS trends a more detailed view of the mixing trends near the cavity and downstream of the injector is also shown in Figs. 8 and 9, respectively.

It is clear from the figures that the RANS and URANS simulations give near-identical predictions of mixing efficiency. The URANS result predicts slightly lower mixing inside the cavity and slightly higher mixing downstream of the cavity compared to the RANS result but the differences are very small, on the order of $\sim$0.4% relative to the RANS result. Further Examination of the URANS trends reveals that values of mixing efficiency continue to change slightly over time after the flow has established, although the differences grow smaller as time increases. This agrees with the observation from Fig. 4 that static pressure inside the cavity is approaching a constant value.

Figures 10 and 11 show trends of total pressure and jet penetration, respectively, for the RANS simulation and the same three time steps of the URANS simulation.

The trends obtained from the RANS and URANS simulation are again near-identical. The URANS results predict slightly higher jet penetration downstream of the injector than in the RANS case, whereas there are no clearly distinguishable differences in total pressure predictions. The maximum relative difference

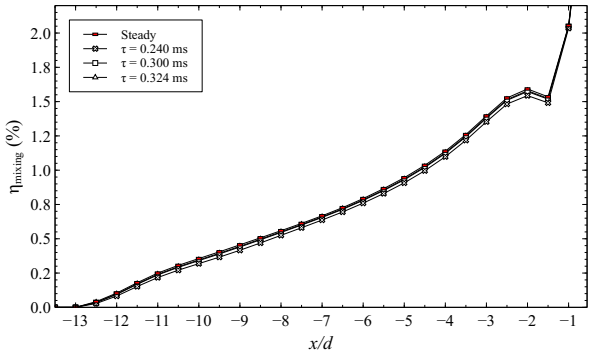

Fig 8. Mixing efficiency in the vicinity of the cavity for three timesteps and the steady case.

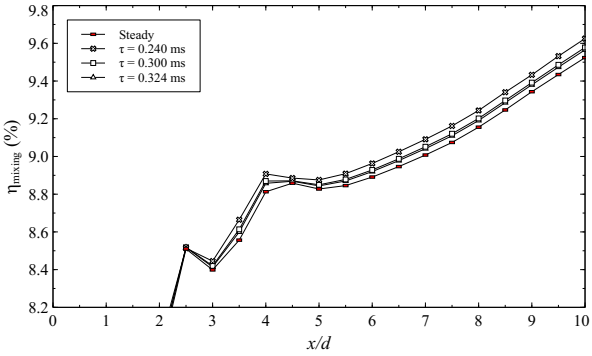

Fig 9. Mixing efficiency downstream of the injector for three timesteps and the steady case.

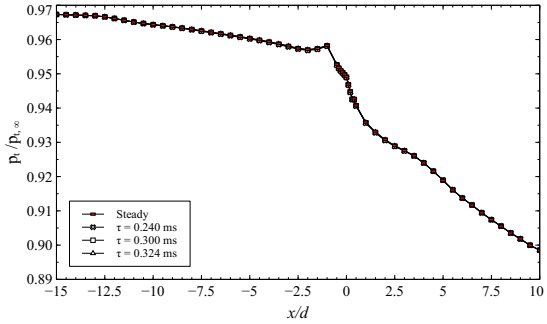

Fig 10. Total pressure through the domain for three timesteps and the steady case.

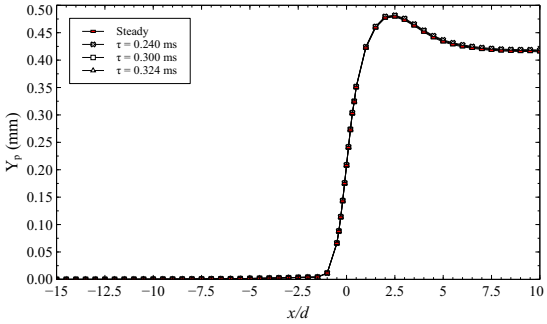

Fig 11. Jet penetration through the domain for three timesteps and the steady case.

between the URANS and RANS results is $\sim$ 0.0012% for total pressure and $\sim$ 0.32% for vertical jet penetration, which is again very small, demonstrating that both simulation approaches predict near-identical one-dimensional flowfield behaviour.

3.3. Effect on flowfield

To examine the effect of unsteadiness on the rectangular upstream cavity flowfield Fig. 12 compares contours of H_2 mass fraction at several streamwise locations for the RANS and URANS result. While the macro plume structure is the same for both simulations, there are slight differences in vertical jet penetration and the fuel distribution inside the plume; the plume is slightly more diffused in the URANS result, as indicated by smaller regions of high H_2 mass fraction in Fig. 12. This is consistent with higher predicted values of mixing efficiency downstream of the cavity in the URANS result,Fig. 9. Jet penetration is also slightly higher in the URANS result because of the higher predicted diffusion, again matching the result observed from the one-dimensional variables. Despite these minor differences the macro jet structure and the development of the jet plume is the same for both cases.

To examine the effect of simulation approach on the cavity flowfield Fig. 13 shows contours of H_2 mass fraction on the combustor wall in the vicinity of the injector for the URANS and RANS simulations.

As before the URANS simulation is observed to be slightly more diffusive; the fuel diffuses farther upstream in the cavity in the URANS result and the low-fuel concentration region at $x/d = -0.5, z/d = -2$ just downstream of the cavity aft wall is slightly smaller. There is also less fuel on the combustor wall from $x/d = 8$ on, after the jet has attached to the combustor wall, which is consistent with the observation from Fig. 12.

While the precise location of the maxima and minima of H_2 mass fraction differs slightly between the

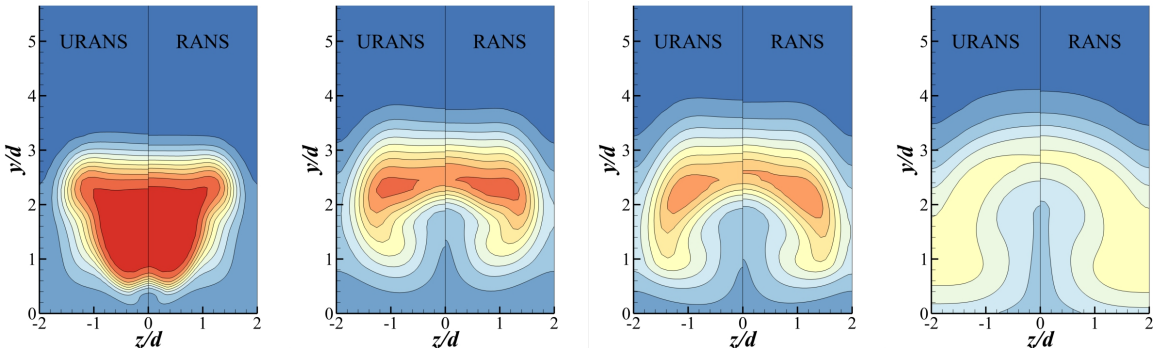

(a) x/d=1 **(b)** x/d=3 **(c)** x/d=4 **(d)** x/d=8

Fig 12. Slices showing contours of H_2 for the RANS and URANS (τ =3 $\times$ 10^{-4} s) simulations at several downstream locations.

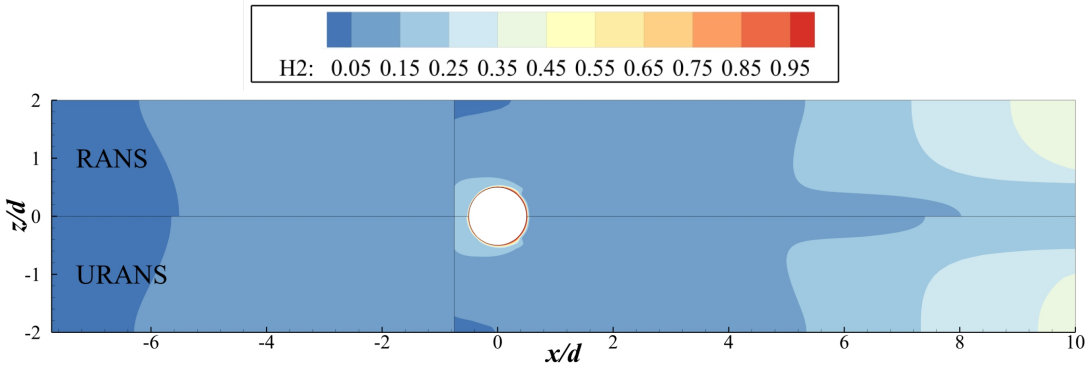

Fig 13. Contours of H_2 on the combustor and cavity wall for the RANS and URANS (τ =3 $\times$ 10^{-4} s) simulations.

two cases, the general distribution is the same; some fuel is transported upstream of the injector into the cavity to approximately $x/d = -6$, the fuel plume touches the lateral sides of the computational domain and the plume attaches to the combustor wall at approximately $x/d = 10$. This demonstrates that the predicted cavity flowfield is very similar for both simulation approaches.

Finally, trends of wall static pressure, wall heat flux and wall H_2 mass fraction at $z/d = 1$ are shown in Fig. 14 to assess how each numerical approach captures local flowfield phenomena such as shocks, separations and attachments.

The trends predicted by the RANS and URANS simulations are largely the same, with slight differences in the predicted value of local extrema. Both simulations predict the same events at the same locations however, indicating that they predict similar flowfield structures and behaviour. This is especially the case inside the cavity, where there is little to no disagreement between RANS and URANS results. Downstream of the injector there are slight larger differences due to slight differences in modelling of the jet plume, as discussed earlier. As downstream distance increases the discrepancy in H_2 mass fraction is observed to grow larger in Fig. 14c, indicating that the discrepancy will grow as downstream distance increases. The effect on one-dimensional mixing efficiency is negligible however, as shown in Fig. 9, likely because the trend in Fig. 14c only captures H_2 mass fraction at a single lateral location, whereas mixing efficiency is calculated over a full streamwise slice.

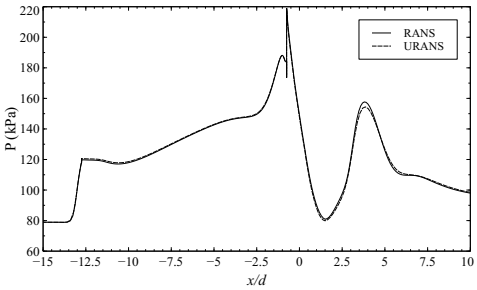

(a) Wall pressure.

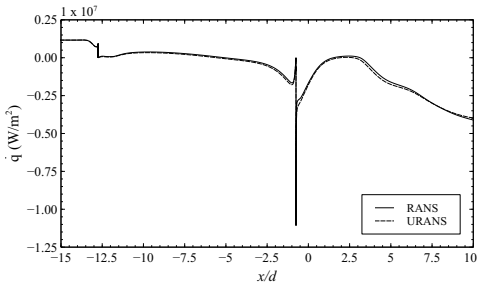

(b) Heat flux.

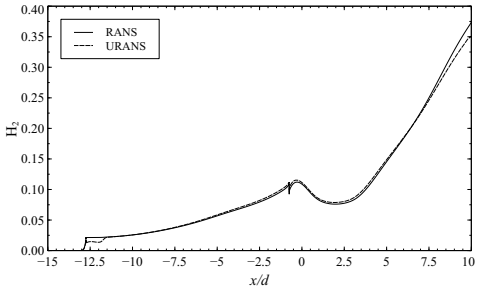

(c) H_2 mass fraction.

Fig 14. Trends of wall pressure (a) wall heat flux (b) and H_2 mass fraction on the wall at $|z/d| = 1$ in the vicinity of the cavity for the RANS and URANS (τ =3 $\times$ 10^{-4} s) simulations.

4. Conclusion

The present study compares URANS and RANS simulations of a scramjet combustor with a novel upstream cavity arrangement. Previous analysis of the RANS flowfield suggested that the upstream cavity flowfield could be steady in nature, even though conventional open cavity flows are well known to be oscillatory in nature. To test the hypothesis of a steady flowfield the upstream cavity configuration was simulated using both URANS and RANS and the predicted flowfields were compared in detail.

Probing of the flowfield showed that once the flow had established no discernible unsteadiness was present inside the cavity; pressure was probed at six locations around the cavity and the cavity shear layer, including the region that drives oscillation in conventional cavity flow, and pressure was found to be constant once the flow had established. Large-scale oscillations are thought to be absent for two reasons: 1) the primary mechanism causing cavity flowfield oscillations is absent in the upstream cavity flow, as the cavity shear layer is lifted over the cavity aft wall and 2) the combustor Mach number ($M = 4.33$) is in excess of the Mach number at which cavity oscillations have been experimentally observed to disappear ($M = 3.2$), due to dampening of shear layer instabilities.

Further examination of the flowfield around the cavity showed that the URANS simulation is slightly more diffusive than the RANS simulation, increasing fuel plume area, however general plume shape and plume development were the same for both simulations. Examination of wall pressure, heat flux and fuel mass fraction trends on the domain wall also revealed that both simulations gave near-identical predictions of the occurance of flow phenomena such as separations, attachments and shocks, with only slight differences in the predicted values of local extrema.

Despite these minor differences, the RANS and URANS simulations were found to yield near-identical trends of one-dimensional performance variables through the domain. Differences in predicted mixing efficiency were on the order of $\sim$0.4% while differences in total pressure and vertical jet penetration were on the order of 0.001% and 0.37%, respectively. This indicates that while minor differences in the flowfield can be present, this does not greatly influence the one-dimensional characteristics and mixing

performance of the flowfield.

These results demonstrate that large scale unsteadiness is absent in the upstream cavity flowfield and that it is valid to use RANS to assess the one-dimensional performance and macro flowfield behaviour of these flows; RANS can capture all relevant flow features that influence the one-dimensional performance and behaviour of the flowfield, while saving computational resources.

Acknowledgements

The authors would like to gratefully thank the support of the CRC-P50510 Hydrocarbon Fuel Technology for Hypersonic Air Breathing Vehicles and RMIT University, as well as the high performance computing resources and support from the National Computational Infrastructure (NCI) Australia. The CRC Programme support industry-led collaborations between industry, researchers and the community.

References

[1] A.N. Antonov, A.N. Vishnyakov, and S.P. Shalaev. "Pressure Pulsations in a Recess over which a Subsonic or Supersonic Gas Stream Flows". In: *Journal of Applied Mechanics and Technical Physics* 22.2 (1981), pp. 215–222.

[2] R.A. Baurle and M.R. Gruber. "A Study of Recessed Cavity Flowfields for Supersonic Combustion Applications". In: *36th Aerospace Sciences Meeting & Exhibit*. AIAA 98-0938. 1998.

[3] A. Ben-Yakar and R. Hanson. "Cavity Flame-Holders for Ignition and Flame Stabilization in Scramjets: An Overview". In: *Journal of Propulsion and Power* 17 (2001), pp. 869–877.

[4] I.B. Celik, U. Ghia, P.J. Roache, et al. "Procedure for Estimation and Reporting of Uncertainty due to Discretization in CFD applications". In: *Journal of Fluids Engineering* 130.7 (2008), pp. 0780011–0780014.

[5] *CFD++ Ver. 17.0 Users Manual*. Metacomp, Inc. Agoura Hills, CA, 2017.

[6] H.H. Heller and J. Delfs. "Cavity Pressure Oscillations: The Generating Mechanism Visualized". In: *Journal of Sound and Vibration* 196.2 (1996), pp. 248–252.

[7] H.H. Heller and D.B. Bliss. "Flow-Induced Pressure Fluctuations in Cavities and Concepts for their Suppression". In: *AIAA Aeroacoustic Conference, NASA Langley Research Center, Hampton, Virginia*. 1976.

[8] H.H Heller, D.G. Holmes, and E.E. Covert. "Flow-Induced Pressure Oscillations in Shallow Cavities". In: *Journal of Sound and Vibration* 18.4 (1971), pp. 545–553.

[9] C.J. Jachimowski. *An Analysis of Combustion Studies in Shock Expansion Tunnels and Reflected Shock Tunnels*. NASA Technical Paper TP-3224. Langley Research Center, 1992.

[10] R.M. Kirchhartz. "Upstream Wall Layer Effects on Drag Reduction with Boundary Layer Combustion". PhD thesis. The University of Queensland, 2009.

[11] R.M. Kirchhartz, D.J. Mee, R.J. Stalker, P.A. Jacobs, and M.K. Smart. "Supersonic Boundary-Layer Combustion: Effects of Upstream Entropy and Shear-Layer Thickness". In: *Journal of Propulsion and Power* 26.1 (2010), pp. 57–66.

[12] S.-H. Lee. "Characteristics of Dual Transverse Injection in Scramjet Combustor, Part 1: Mixing". In: *Journal of Propulsion and Power* 22.5 (2006), pp. 1012–1019.

[13] L.-Q. Li, W. Huang, and L. Yan. "Mixing Augmentation Induced by a Vortex Generator Located Upstream of the Transverse Gaseous Jet in Supersonic Flows". In: *Aerospace Science and Technology* 68 (2017), pp. 77–89.

[14] F.R. Menter, M. Kuntz, and R. Langtry. "Ten Years of Industrial Experience with the SST Turbulence Model". In: *Turbulence, Heat and Mass Transfer* 4.1 (2003), pp. 625–632.

[15] *Pointwise V18.0 User Manual*. Pointwise, Inc. 2017.

[16] A.S. Pudsey, R.R. Boyce, and V. Wheatley. "Influence of Common Modelling Choices for High Speed Transverse Jet Interaction Simulations". In: *Journal of Propulsion and Power* 29.5 (2013), pp. 1079–1086.

[17] T. Roos, A.S. Pudsey, M. Bricalli, and H. Ogawa. "Cavity Enhanced Jet Interactions in a Scramjet Combustor". In: *Acta Astronautica* 157 (2019), pp. 162–179.

[18] T. Roos, A.S. Pudsey, M. Bricalli, and H. Ogawa. "Numerical Investigation of Upstream Cavity Enhanced Combustion in a Scramjet Combustor". In: *23rd AIAA Hypersonics and Spaceplanes Conference*. AIAA 2020-2429. 2020.
[19] T. Roos, A. Pudsey, H. Ogawa, and M. Bricalli. "Numerical Investigation of Upstream Cavity Enhanced Fuel Mixing in Scramjet Combustors". In: *Acta Astronautica* 169 (2020). To be published, pp. 50–65.
[20] J.E. Rossiter. *Wind Tunnel Experiments on the Flow Over Rectangular Cavities at Subsonic and Transonic Speeds*. Tech. rep. 3838. Ministry of Aviation; Royal Aircraft Establishment; RAE Farnborough, 1964.
[21] O.H. Unalmis, N.T. Clemens, and D.S. Dolling. "Experimental Study of Shear-LayerAcoustics Coupling in Mach 5 Cavity Flow". In: *AIAA Journal* 39.2 (2001), pp. 242–252.
[22] H. Wang, P. Li, M. Sun, and J. Wei. "Entrainment Characteristics of Cavity Shear Layers in Supersonic Flows". In: *Acta Astronautica* 137 (2017), pp. 214–221.
[23] D.C. Wilcox. *Turbulence Modeling for CFD*. La Canada, CA: DCW Industries, Nov. 1994.
[24] X. Zhang and J.A. Edwards. "An Investigation of Supersonic Oscillatory Cavity Flows Driven by Thick Shear Layers". In: *The Aeronautical Journal* 94.940 (1990), pp. 355–364.
[25] X. Zhang and J.A. Edwards. "Experimental Investigation of Supersonic Flow over Two Cavities in Tandem". In: *AIAA Journal* 30.5 (May 1992), pp. 1182–1190.
[26] X. Zhang, A. Rona, and J.A. Edwards. "The Effect of Trailing Edge Geometry on Cavity Flow Oscillation Driven by a Supersonic Shear Layer". In: *The Aeronautical Journal* 102.1013 (1998), pp. 129–136.